A new physics-based NBTI model for DC-and AC-stress enabling accurate circuit aging simulations considering recovery

Christian Schlünder, Hans Reisinger, Wolfgang Gustin, Tibor Grasser*

Infineon Technologies AG, D-81726 Munich, Germany, *Institute for Microelectronics, TU Wien, Wien, Austria
Tel: +49 89 234 52934, Fax: +49 89 234 9557544, Email: christian.schluender@infineon.com

Abstract

Aging circuit simulators require a correct and not too complex device degradation model for accurate aging predictions. But the physical origin of the Negative Bias Temperature Instability (NBTI) as the most important device degradation mechanism is still not fully understood and under debate. Especially the recovery- and accordingly the AC-stress-behavior are not mapped correctly by current commercial aging simulators. In this work we present and verify a new, physics-based, quantitative model allowing a precise prediction of NBTI degradation and recovery. This model takes the stress history into account and also provides a prediction for degradation due to AC-NBTI and an understanding of the special features seen in conjunction with AC-NBTI. As groundwork we analyze the single defects constituting NBTI. A new measurement technique stimulating a controlled discharge of these defects will be introduced. By employing a statistical analysis of many stochastic stimulation processes of the same defect we are able to determine the electric field and the temperature dependence of these defects with great precision. This new understanding and model can build the base for an accurate aging circuit simulation integrated within the standard design flow. Lifetime enhancement due to recovery during stress intermissions and/or during AC-stress can be calculated with high precision.

INTRODUCTION

The very fast recovery behavior of NBTI complicates parameter extraction and lifetime estimations for reliability evaluations of CMOS technologies. On the other hand the recovery of the parameter degradation offers enormous lifetime enhancement, if the stressed devices find recovery during product lifetime. Time periods in non-stress or reduced stress conditions and even an AC-stress leads to parameter drift relaxation down to a possible full recovery.

Exploitation of recovery for lifetime estimations is rather difficult, since the lifetime enhancement have to be calculated correctly and worst case stress scenarios without recovery have to be identified. An aging circuit simulator can solve this problem as soon as the deposited degradation model can handle it [1-3]. Fig. 1 shows a comparison between a state-of-the-art commercial aging simulator [25] and a real measurement. An AC-stress signal is applied and the parameter degradation is extracted in steps. While the degradation behavior is modeled satisfactorily, a huge error up to 100% for the predicted recovery can be obtained between the simulator estimation and the measurements. Also other groups report inadequateness of the recovery model within the aging simulator [15]. The NBTI recovery is considerably underestimated. This relies among other things on several points:

- The simulator uses a not physics-based model.
- The distribution of time constants of the NBTI contributing defects is not captured.
- The model does not consider the sample's stress-history
- The AC-NBTI behavior is not modeled correctly

In the following, each point will be explained in detail and possible solutions suggested. As groundwork for an accurate model the physics behind NBTI have to be understood as accurately as possible. The mechanism of each single defect contributing to NBTI has to be illuminated.

NBTI ORIGIN

Even after many years of research [4] we still have no consensus regarding the physical origin of NBTI. So far only electron spin resonance (ESR) experiments [5] have provided some insight into the microscopic processes. The majority of electrical experiments have been done on large pFETs and thus averages over many defects (see table 1). We will show that this averaging obscures the properties of the individual defects and leads to misinterpretations, for example of the thermal activation. In this work we analyze the properties of the single, discrete events constituting NBTI degradation and recovery in small FETs. We have developed analysis techniques based on those known from the Random Telegraph Signal (RTS) studies of the 1980s [6, 7]. RTS is caused by capture and emission of charge in oxide traps. RTS studies have been done predominantly nMOSFETs [7], the FETs kept in a quasi steady state. In contrast, our method uses multiple high-gate-field charging pulses to excite the defect state to a charged state.

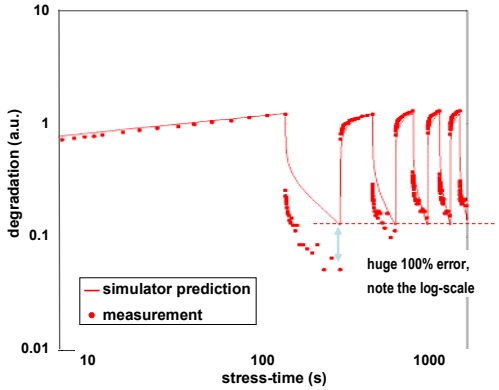

Fig. 1: Comparison between the calculated simulator prediction of NBTI parameter degradation and real measurement. For AC-stress a huge deviation up to 100% error can be obtained. The simulator overestimates the degradation by far.

This technique is similar to the deep level transient spectroscopy (DLTS) [9], but it is essential to vary the length of the charging pulses, because of the wide distribution of capture time constants. This is why we term the technique time dependent defect spectroscopy (TDDS).

Stimulated by recent work on small pFETs [8, 10] we employ a new highly accurate extraction scheme for NBTI-relevant defect parameters. Capture and emission time constants τ_c and τ_e, (corresponding to stress and recovery) have been seen before [10, 11]. However, to extract temperature- and field-dependencies of those τ_cs and τ_es, and thus to gain insight in physical processes, a highly accurate determination of averaged time constants is required. Thus we extract averaged values for τ_c and τ_e from repetitive measurements. Typically 100 or more excitations and measurements are done for each τ_c and τ_e determination for a given defect and condition. Main parameters are the gate voltage, the length of the excitation pulse and the temperature.

SAMPLES AND EXPERIMENTS

We use pFETs with a 2.2nm nitrided oxide. The geometries were small enough to conveniently resolve the effect from a single carrier in the channel (typical ΔVT=1mV, see table 1) and large enough to have at least a handful of active defects (≈20 average step-height defects for ΔVT=20mV). The values of table 1 were calculated with a simple charge-sheet model and thus give only average step heights in *VT*. The variations of the listed step hights and their origin in FETs of a similar geometry are explained in [17].

In order to occupy individual defects, a stress pulse was applied to the gate. To determine the different capture time constants, stress pulses ranging from 200ns to 100s were employed. ΔVT was directly recorded after the pulse for a time of typically 1000s, using our fast feedback loop. For a detailed description of our measurement technique please refer to [12, 14]. Each pulse-readout-sequence was done repetitively (32 to 256 times) to allow for a statistical analysis. A rough determination of individual capture and emission times (e.g. within a factor 2, like in Fig. 3) could be done by recording just a few traces. However, if precise parameter dependencies (on *Vgate*, or *T*, cmp. Fig. 8) are required, a statistical analysis of many traces has to be done. To ensure the same pre-pulse condition for each pulse/readout sequence, full recovery had to be awaited after each stress pulse (cmp. Fig. 5). A measuring sequence for a given gate voltage and temperature, just varying the stress pulse width from 1µs to 10s, requires several days. All information, also about capture, is gathered during recovery. The total number of carriers in the channel of a minimal short/narrow FET is under stress in strong inversion by a factor of 10 higher than during the recovery phase (ca. 200:2000 carriers). Therefore the effect of a single carrier on the drain current is by a factor of 10 smaller. While 0.5% change can be measured accurately, 0.05% is below the noise level in general. Thus an extraction under stress is not possible.

FET-name and dimension (in µm)	wide		narrow		minimal	
	W	L	W	L	W	L
	10	**0.1**	**0.2**	**0.12**	**0.11**	**0.1**
number of carriers in channel at Vg=VT-200mV	**15000**		**370**		**170**	
number #Nit at a density DNit=1E11/cm^2	**1000**		**24**		**11**	
ΔDNit causing a ΔVT=50mV (in cm^{-2})	**4.9 x 10^{11}**		**4.9 x 10^{11}**		**4.9 x 10^{11}**	
makes a number Δ#NIt	**4900**		**120**		**50**	
ΔVT caused by a single trapped carrier (at interface)	**0.01mV**		**0.43mV**		**1.0 mV**	

Table 1: Geometries of the used pFETs and some useful numbers. Oxide thickness is 2.2nm. Measured specific capacitance in inversion is 1.3µF/cm^2. Real measured step-heights for the minimal FET (cmp. underlined value) range from 0.2mV to 5mV. DNit denotes the charged interface-states density.

COMPARISON WIDE AND NARROW FET

Figs. 2 and 3 show that NBTI degradation and recovery in wide and narrow FETs are equivalent. Degradation in the narrow FETs is 30% higher than in the wide FET, presumably due to edge/stress effects (e.g. shallow trench isolation (STI)).

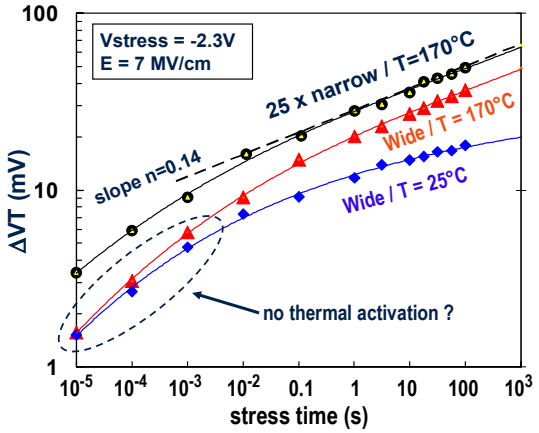

Figure 2. Comparison of degradation for a narrow (0.2µm) and a 10µm wide FET at 170°C. The narrow FET data is from summing up 25 single 0.2µm wide FET data. For the wide FET the thermal activation, and the "missing" thermal activation for µs to ms times are shown.

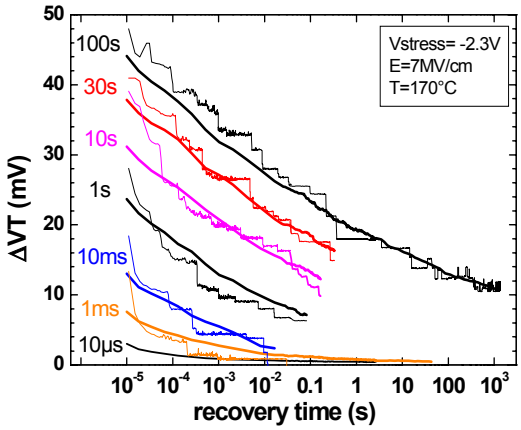

Figure 3. Comparison of the recovery traces for a single narrow (traces with steps) and the average over 25 different 0.2µm wide FETs (smooth traces). Labels denote the stress time preceding the recovery trace. The recovery behavior of the wide devices (see Fig. 2 in ref.[19]) is identical to the narrow FETs.

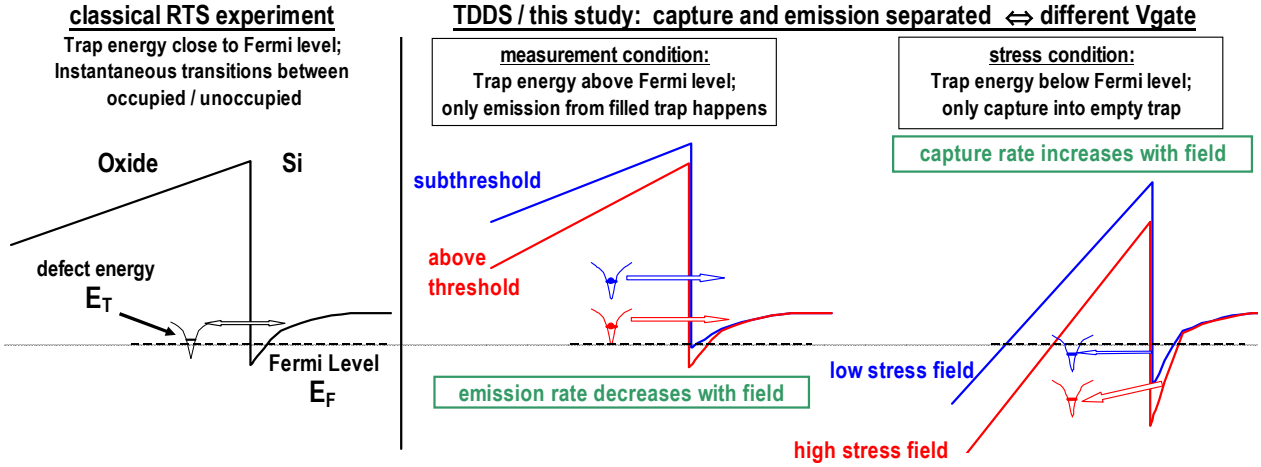

Figure 4. Schematic band-diagrams, showing the inversion layer and defect levels in the oxide in the vicinity of the substrate. The diagram is meant to be polarity independent, showing the conduction band in an nMOSFET **or** the valence band of a pMOSFET when flipped upside down. Increasing potential energy corresponds to the upward direction. States above / below E_F are empty / occupied, respectively. Each of the 3 diagrams contains the same **single trap** shown for **two different fields** (red/blue) on the TDDS-side of the diagram. Arrows just indicate the charge carrier transitions between an initial and a final state. These arrows are **not supposed** to indicate that the charge transfer process is due to elastic or inelastic tunneling. In contrast the charge transfer is thermally activated for all cases, including RTS. RTS and TDDS do not differ with respect to sample type, nature of traps or physical processes involved. The main difference for TDDS is the stimulation of capture at a field higher than the field for emission, and the way of data analysis. **The capture rate** increases with increasing field. **Emission rate** increases with decreasing field.

This observed geometry dependence is consistent with the literature [18]. In the narrow FETs all *VT* changes consist of discrete steps from individual defects. After averaging over a large number of small FETs the curves are as smooth as from wide-FETs (cmp. Fig. 3). Each defect causes a specific step-height, which allows for the identification of individual defects as shown in Fig. 5.

PHENOMENOLOGICAL MODEL

For a basic understanding of our results the model by Kirton/Uren [4] for random telegraph signals (RTS) is used. A major issue of the model is its failure to properly predict the bias dependence of capture and emission, see [13] for a discussion. A model sketching the band diagrams corresponding to capture and emission is given in Fig. 4. We want to stress that Fig. 4 is simplified and meant only to illustrate the basic properties of capture and emission of charge. It does not show the energy barriers corresponding to structural relaxation in any way. A model which treats the microscopic physical processes is presented in [13]. The transitions neither in classical RTS nor in our data are explainable by elastic tunneling. Instead the capture and emission of charge carriers involves a structural relaxation of the oxide matrix surrounding the defect. Thus a transition requires, like in a chemical reaction, an overcoming of a barrier by **heavy** particles. As a consequence the transitions are thermally activated. Since the energy level of the charged defects is field dependent, the reaction rate for both directions, capture and emission of charge is gate voltage dependent. The experiments in this work and also low temperature experiments [16] have clearly shown that tunneling of light particles (electrons or holes), which is nearly temperature independent, does not contribute to NBTI.

STATISTICAL ANALYSIS OF AN INDIVIDUAL DEFECT

An example for the defects' response of roughly 10 defects to stress pulses is given in Fig. 5. For the *ts*=10ms traces only a single medium-to-slow defect happens to be active. The stress field has led to capture of a hole by pulling its energy level E_T (see Fig. 4) far below E_F, thus its occupancy level is nearly unity after stress $ts>\tau_c$. Note that the valence band in Fig. 4 is flipped upside down in order to have rising energy up and occupied levels below E_F.

After the stress is released (*ET* above *EF* again, equilibrium occupancy level ≈0) it will be discharged by emission (like radioactive decay) at a random time around a characteristic emission time τ_e. Averaged over many emission events (see Fig. 7) the defect's occupancy will decay with recovery-time *tr* following $\boldsymbol{Occ=exp(-tr/\tau_e)}$. The same statistical behavior describes the **capture** of a hole during stress.

Occupancy during stress time *ts* increases like $\boldsymbol{Occ=1-exp(-ts/\tau_c)}$. τ_c is determined from the measured average occupancy level after many stress pulses with *ts* around τ_c as shown in Fig. 6. In Fig. 7 the temperature dependence of τ_e of a given defect is investigated. Each emission time of this defect, extracted from a recovery trace, is plotted as a dot, allowing to extract τ_e corresponding to the slope of a straight line. The fit to the straight line also is a proof that the defects behave in the expected statistical way and that **only one** defect is contained in the distribution. Mixing another defect into the distribution, by chance with a similar step-height, which would be hardly to distinguish, would lead to a deviation from the straight line. In order to minimize the statistical error in the determination of τ_c the stress pulse width *ts* has to be chosen to have a similar value as τ_c. As seen in Fig. 6 *ts* increasing in steps of a factor 10 delivers a satisfactory accuracy for all τ_cs. Fig. 8 shows extracted τ_cs and τ_es for a couple of defects as an

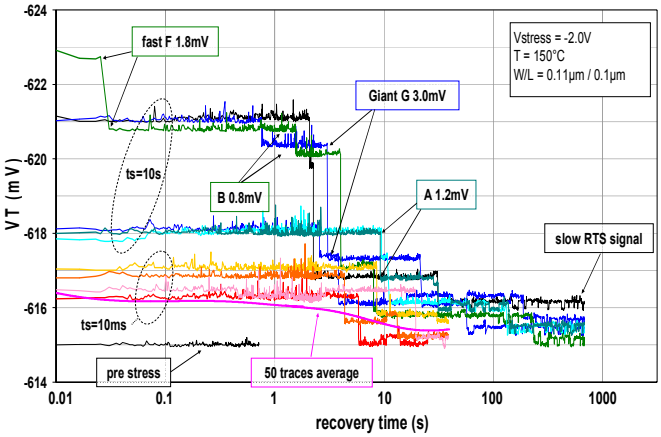

Figure 5. An example of steps from emission of positive charge from defects during recovery, all from the same device. Stress pulses are applied repetitively (typ. 100 times). Some traces, 4 after 10ms stress-pulses (reddish color) and 6 after 10s stress (bluish) were chosen as examples. Individual defects can be distinguished by their step heights, allowing to name the traps, A, F, G, etc. The smooth trace is an average over 50 traces showing the exp(-t/τ_e) behavior.

Arrhenius plot. Our statistical analysis allows a very precise determination of activation energies E_A. E_As are higher than the ones extracted from conventional experiments, but in agreement with the findings from ultra-fast temperature changes [20]. We will discuss these E_As again in section "The missing-thermal-activation riddle". It should be noted that the thermal activation of the single defects show no deviation to an Arrhenius behavior (cmp. Fig. 8), in contrast to a conventional determination of thermal activation done on wide FETs [21]. This work shows only one example for parameter extraction, namely the T-dependence determination in Figs. 6, 7, 8. In an analogous way also the *Vgate* dependence of τ_cs and τ_es can be determined. These results are presented in [13].

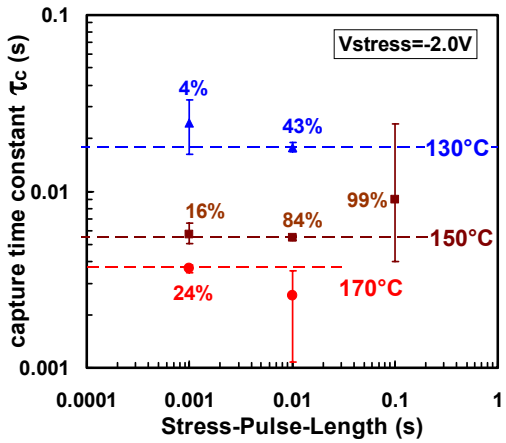

Figure 6. Example for the statistical analysis of capture time constants from repetitive capture attempts (by doing stress pulses of 1ms, 10ms and 100ms) for a single defect at 3 temperatures. Labels denote the capture probability, equal to the ratio r=number capture events / number of attempts. Note that r is the quantity which is directly measured. As can be seen, the statistical errors (see error bars) in the determined τ_c can be minimized, or at least kept small by choosing the stress pulse length suitable to have the capture probability between 15% and 90%.

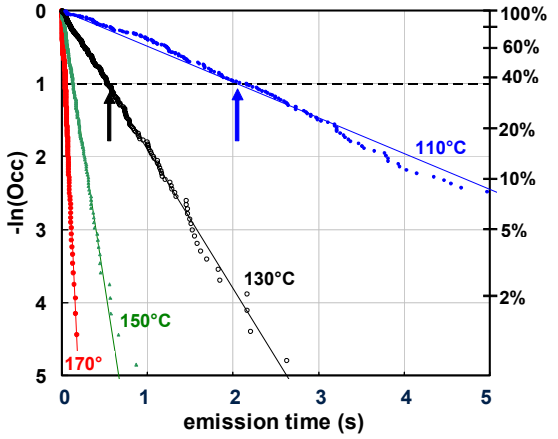

Figure 7. Example for the statistical analysis of emission times of a single defect at 4 temperatures. Plotted is the decreasing occupancy of a defect, starting with 100% just after capture, i.e. at zero emission time. Arrows mark the time constants τ_e. The straight line behavior demonstrates that only a single defect is contained in each curve. Each dot corresponds to an emission event in a recovery trace like in Fig. 5.

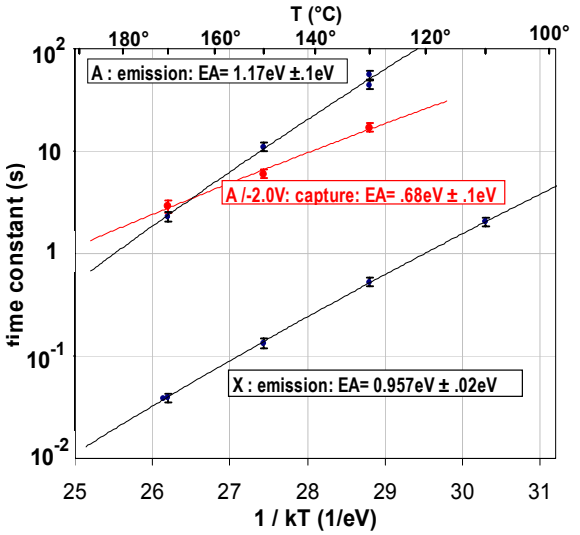

Figure 8. Arrhenius plot for defect A as well as capture and emission for trap X. E_A values are higher than in conventional experiments. Note the considerable accuracy in determining τ values. Each point is extracted from 256 emission events of the given defect.

New NBTI Model

With the findings so far we can be sure that the model of distributed time constants as proposed in [10] correctly describes the recoverable part of NBTI. An equivalent circuit for the model is shown in Fig. 9. Each defect is represented by a capacitor C which can be charged or discharged from a signal line applying stress- or recovery-voltage. The charge or voltage on C is equivalent to the individual ΔVT caused by the defect. The complete model for a FET thus consists of just one RC-element for each defect. The value of C for each defect will be roughly the same and corresponds to the value of ΔVT produced by this defect. The values for the charging resistor R_c and the discharging resistor R_e determine the capture and

emission time constants R_cC and R_eC and are widely distributed. All the time constants are a function of *Vgate* and temperature. We will employ this NBTI model in the following sections.

THE MISSING-THERMAL-ACTIVATION RIDDLE

Short-term degradation is sometimes found to be apparently T-independent (see wide FET in Fig. 2). This has led to the assumption that short-term NBTI is due to elastic QM-tunneling. In strong contrast, **all** the capture/emission events we analyzed, for <1µs up to ks, were strongly thermally activated (cmp. Fig. 7). An explanation is given in Fig. 10: Thermal activation is equivalent to shifting an RC-ladder - extended quasi-infinitely to short and long times - up or down (25°C to 170°C means ≈4 decades in time). It is clear that this shift has **no effect** when τ_c and τ_e (i.e. degradation and recovery) are both thermally activated by a similar *EA* and when τ_c and τ_e - though $\tau_c \neq \tau_e$ - are both evenly distributed on a log-time-scale (as known to be the case for short times).

PRACTICAL MODELING

A distribution map of defect properties based on few defects is shown in Fig. 11. Clearly this map does not contain a number of defects large enough to be representative for a "real", say 0.5µm-wide FET. A 0.5µm wide FET would have filled ≈250 defects at a ΔVT=50mV (cmp. table 1). To fill this map with >250 measured defects in order to get a modeling-relevant spectral-density-map would be a task taking at least months. However, with our new understanding of trap properties, we now have the justification to switch back to a wide FET (with >4000 defects) and can extract a full defect density map just from measuring full-recovery traces from a single FET. This justification is mainly based on the fact that the number of defects and their properties do not change during stress (see also points 2, 3, 4, 5 in the conclusions). The principles of extracting such a map, of gathering all the information needed, are outlined in Figs. 12 and 13. The "difference"-curve actually is a recovery curve containing all defects having a capture time constant between 10ms and 100ms.

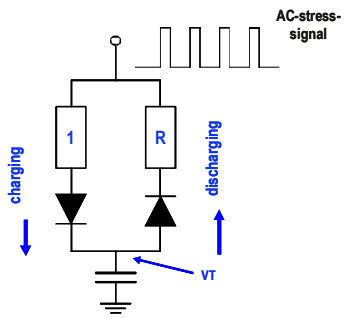

Figure 9. A single RC-element representing one given defect with a capture and emission time constants τ_c and τ_e having a ratio τ_e / τ_c =R. The voltage *VT* on C corresponds to the ΔVT produced by this defect. A real FET contains a large number of these defects (see Fig. 13) , the individual *VT*s have to be summed up. The signal applied to the upper terminal indicates charging of the RC-element by an AC stress.

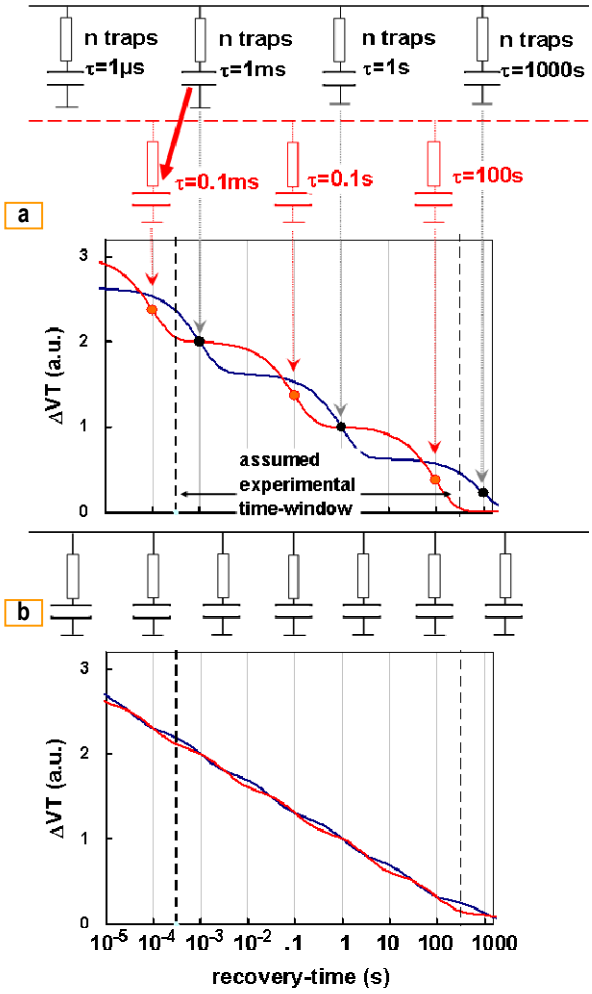

Figure 10. Simplified simulation of NBTI using the equivalent circuit from the top of the Figure. The τ's are aligned with the X-axis. When the τ's are widely separated (only one in 3 decades in Fig. a) distinct bumps are produced. A change of τ (by increased temperature, indicated by the red arrow) shifts the distinct bumps in the recovery curves. With densely, equally distributed RC's, ranging from 1ns to 1Ms (Fig. b) it is obvious that a shift left/right of this ladder has **no effect** in the experimental time window.

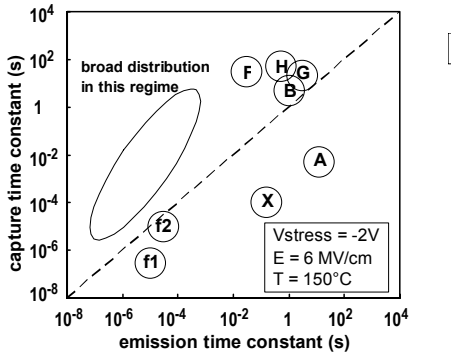

Figure 11. Correlation of τ_c/τ_e of a couple of selected defects from the statistical analysis of single defects (cmp. Fig. 5). τ_e may be larger or smaller than τ_c by orders of magnitude.

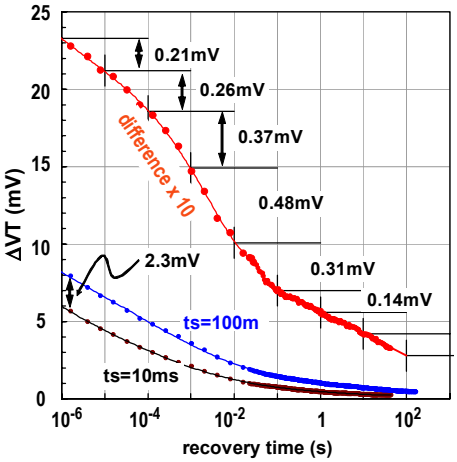

Figure 12. Example for extraction of spectral trap densities from recovery traces: The difference between ts=10ms and ts=100ms traces is due to the class of defects with 10ms<τ_c<100ms. So this class can be separated and then divided into "bins" of different τ_e s (i.e. recovery times). Experimental parameters are given in Fig. 14.

All these defects then are separated in one-decade-wide bins of different emission time constants as shown in Fig. 13. The filling level of the bins is given simply in mV-units, corresponding to the *ΔVT* generated by each bin. The density levels from Fig. 12 (denoted as labels in Fig. 12 and 13) contain the information to fill just one slice in Fig. 13. The other slices of Fig. 13 are filled in an analogous way. When all the squares in the defect density map Fig. 13 are filled this map comprises a complete set of parameters allowing a complete and straightforward modeling of NBTI for a given stress voltage and temperature. It includes recovery and the response of the sample to AC-stress or to any arbitrary sequence of stress-recovery cycles.

An example for a calculated degradation curve and a recovery-curve in comparison to the experimental curves is given in Fig. 14. As can be seen, the fit is perfect. This is not a surprise, however.

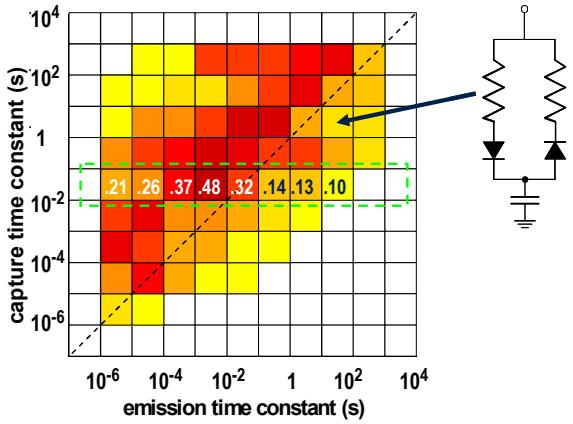

Figure 13. Complete spectral density map. The τ_c-slice analyzed in Fig. 12 is marked by a frame and labeled with the numbers from Fig. 12. Spectral density is simply given in *ΔVT*-units (=mV). The experimental parameters are given in Fig. 14. Each square corresponds to a class of defects with given τ_c and τ_e as indicated by the RC-element.

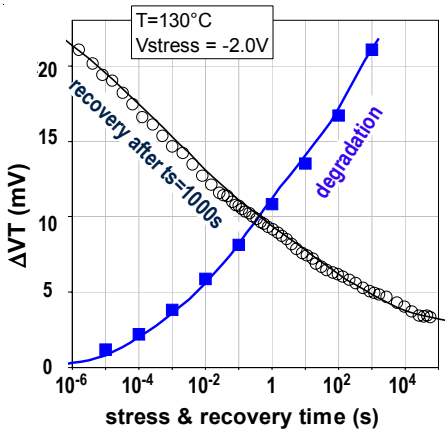

Figure 14. Using the parameter-table given in Fig. 13 a simulation of degradation to ts=1000s and subsequent recovery is done. Dots are experimental points; lines are calculated values.

Our model and the way of parameter extraction actually very much resembles a Fourier transformation: A set of data in the time-domain, (example Fig. 12) is just converted into a set of coefficients in the frequency domain (example Fig. 13), i.e. the set of "amplitudes" in the 2-dimensional spectral plot. Fig. 14 is quasi a re-conversion into the time-domain. If done correctly this re-conversion, like a Fourier transformation exactly reproduces the experimental data as demonstrated in Fig. 14. To prove the claim that the model is able to predict recovery and degradation for any arbitrary stress signal, a further model verification is shown in Fig. 15. Note that the stress condition is different from the example in Figs. 12, 13 and 14.

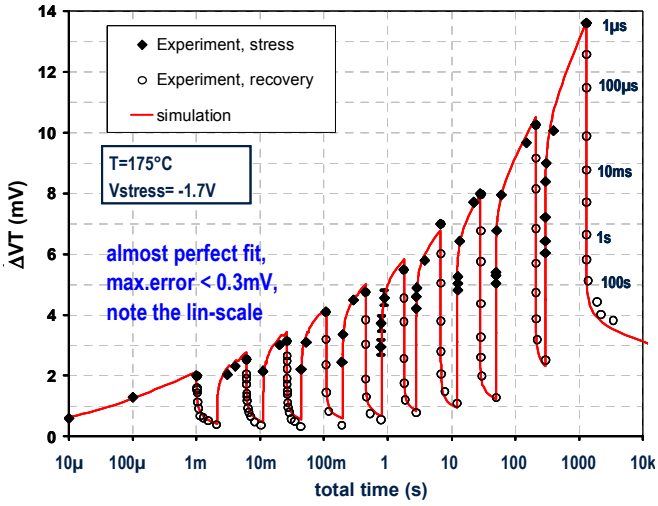

Figure 15. Example for model verification: Vstress is close to the maximum operating voltage of 1.6V. A stress/recovery sequence with increasing times was chosen. Agreement between experiment and model is in the sub-mV regime. Obviously all the experimentally observed time constants from µs to >10^3s are correctly captured by the simulation. Readouts during the stress phases (filled dots) have been measured with a measuring delay of 1µs and a total interruption of stress of 10µs. Measuring delay as well as this interruption are also considered in the simulation. The dents in the simulation, seen between 2ms and 5ms, are due to this interruption. Labels at the rightmost recovery branch denote the recovery time for each point, valid for each of the recovery branches.

For the model verification a series of stress/recovery sequences, with increasing times, has been applied to a sample and then simulated. As can be seen, the quality of fit is very good. Unfortunately the log-time axis obscures all the µs to 1s time effects which are occurring for the long times also. To regain some of this information the experimental points have been chosen to be equidistant on a log-time scale.

In order to give an impression of the time demand for the simulation, the shown results were calculated on a GHz CPU in a range of ms. Thus the model is practicable applicable in contrast to the approach described in ref. [15] requiring minutes for one device.

AC-STRESS

Existing studies about AC-NBTI, e.g. [22] show a relation of *ΔVT* vs. duty cycle having the typical S-like shape. The reason for this shape could not been explained yet. Fig. 16 shows measured AC-stress data in comparison with a very simple simulation. The simulation perfectly fits the experimental data, proving that the AC- behavior can be fully understood by our model. The fit-curve in Fig. 16 is "assembled" from a sum of 3 contributions, corresponding to 3 classes of defects. The 3 classes differ by the ratio between capture- and emission time constant. Class "S" has an emission time constant much slower than capture τe>>τc. Looking at the equivalent circuit it is clear that this is the behavior of an electronic peak detector. The C in the peak detector is almost fully charged as soon as the duty cycle D is just above zero. Class "F" has capture much slower than emission, τc>>τe. It is the opposite of the peak detector. D has to be very close to 100% to get a little charge into C, depending on the value of the ratio τe/τc. Finally class "M" has an emission time equal to capture time. It gives the linear response seen in Fig. 16 and is responsible for the linear center part of the experimental curve. Naturally, the assumption that there are just 3 classes of defects is an oversimplification. Still, the shape of the curve in Fig. 16 is mainly determined by the contributions by the "extreme" classes "F" and "S". Thus the consideration of just 3 classes gives a perfect fit. It is noteworthy that mainly the ratio τc /τe determines the shape of the curve, while the absolute values are not important, as long as these time constants are longer than the AC-period. This explains a good deal of the observed independence of AC-degradation on frequency. Given that the measuring delay is much shorter than the stress-time (in our experiments by more than 5 orders of magnitude) there also is no influence of the measuring delay. In our experiment the ΔVT measurement is always done after the completion of the stress-phase of an AC stress cycle. Measurement and stress signal are synchronized. Like for DC-stress we define the short (2µs) recovery phase before VT is determined as the measurement delay.

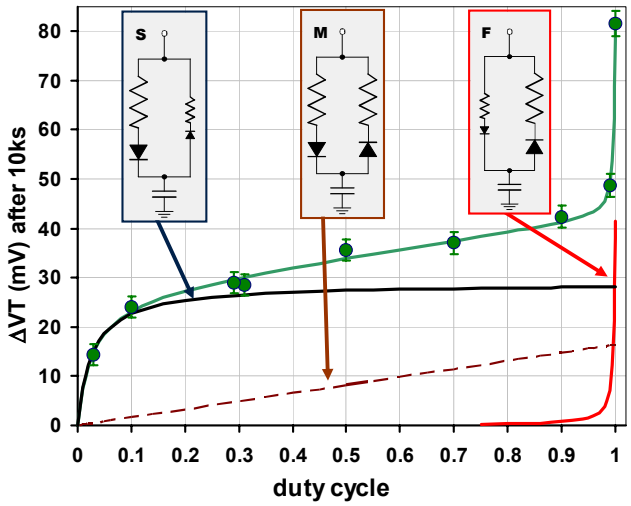

Figure 16. Degradation under AC stress at -2.7V at 175°C / 100kHz as a function of duty cycle. The full line trough the data is a best fit. It is composed as a sum from 3 contributions (the 2 full and the dashed lines), corresponding to 3 types of equivalent circuits S, M, F (=defects) as described in the text. The magnitudes of the 3 contributions are roughly equal.

AC-stress measurements are easy to do, and will provide a lot of information about the sample. An experimental setup with a short measuring delay should be used, and the measurement-timing should be synchronized with the AC-signal. In this work we could only briefly sketch our experimental AC-results, the modeling and the derivations done. It is clear that the calculation of the response of an RC-element with e.g. a 1000s time constant, for a 10 year AC stress, with a total of 1015 AC-periods will need a couple of appropriate approximations in the calculation.

CONCLUSIONS

Based on our new defect spectroscopy technique we were able to resolve some open questions in NBTI. We draw the following conclusions. All these conclusions are based on the experimental observations only and do not require further assumptions or models.

(1) The recoverable part of NBTI is completely driven by pre-existing defects. For a moderate degradation below a $5*10^{11}cm^{-2}$ charge defect density no generation of defects has been observed.

(2) Each defect is characterized by a capture and an emission time constant τ_c and τ_e, both a function of temperature an electric field.

(3) τ_c and τ_e have a wide distribution and are not correlated (see Figs. 11, 13).

(4) Recovery of a given defect is only a matter of defect properties, absolutely independent of the previous stress-time and stress-voltage. This fact rules out that any diffusion is involved in degradation or recovery [23].

(5) Defects charging and discharging events are mostly uncorrelated. This is plausible, because with a density of $10^{12}cm^{-2}$ their typical distance is 10nm which is more than the screening length in the inversion layer [24]. Exceptions are shown in ref. [13].

(6) All processes, also short term 1µs to 1ms, are thermally activated with an activation energy of typically 1eV. As explained in section VI, the seemingly T-independent degradation at short times is an artifact.

(7) The new understanding of NBTI leads to a straightforward model, especially of AC-NBTI, based on a simple equivalent circuit like in Fig. 9 and a set of empiric parameters.

(8) If a defect density map like the one in Fig. 13 describes degradation and recovery, it is clear that the concept of "universal recovery" cannot be correct but at the most an approximation.

Based on the presented new understanding of NBTI, verified by numerous experiments, we were able to present a physics-based, quantitative model, allowing a precise prediction of NBTI degradation and recovery. This model takes the stress history into account and also provides for the first time a prediction for degradation due to AC-NBTI. Based on this model aging simulators will be able to calculate the lifetime enhancements by recovery due to stress intermissions and/or AC-stress.

REFERENCES

[1] Christian Schlünder, "Design for Reliability (DfR) - A key requirement for modern product design"; 3. GMM/GI/ITG-Fachtagung Zuverlässigkeit und Entwurf (ZuE2009), GMM-Fach-bericht, Nr. 61, Sept. 21.-23., Stuttgart, Germany, 2009, p. 19 presentation only, printed version: 4. GMM/GI/ITG-Fachtagung Zuverlässigkeit und Entwurf (ZuE2009) (in press)

[2] T. Pompl, C. Schlünder, M. Hommel, J. Schneider, „Practical Aspects of Reliability Analysis for IC Designs",43rd Design Automation Conference, San Francisco, California, July 24-28, 2006, pp. 193-198

[3] Christian Schlünder, "The NBTI challenge spreading out from technology to design - Design for Reliability", , Tutorial Notes 2007 IEEE International Reliability Physics Symposium (IRPS), Apr. 15th, Phoenix, 2007, pp. 1-18

[4] J. H. Stathis and S. Zafar, "The Negative Bias Temperature Instability in MOS Devices: A Review", MR Vol. 46, no.2-4, 2006, p. 270

[5] J. P. Campbell, P. M. Lenahan, A. T. Krishnan, and S. Krishnan, "Identi-fication of the atomic-scale defects involved in the negative bias tempe-rature instability in plasma-nitrided p-channel metal-oxide-silicon field-effect transistors", J. Appl. Phys., Vol. 103, no. 4, 2008, pp. 044505-1-11

[6] K. S. Ralls , W. J. Skocpol, L. D. Jackel, R. E. Howard, L. A. Fetter, R. W. Epworth, and D. M. Tennant, "Discrete Resistance Switching in Submicrometer Silicon Inversion Layers: Individual Interface Traps and Low-Frequency (1/*f*?) Noise", Phys. Rev. Lett. 52, pp.228-231, 1984

[7] M. J. Kirton and M. J. Uren, "Noise in solid-state microstructures: A new perspective on individual defects, interface states and low frequency (1/f) noise", Adv. Phys., vol. 38, pp. 367-468, 1989

[8] V. Huard, C.R. Parthasarathy, and M. Denais, "Single-Hole Detrapping Events in pMOSFETs NBTI Degradation, 2005 IIRW final report, p. 5

[9] A. Karwath and M. Schulz, "Deep level transient spectroscopy on single, isolated interface traps in field-effect transistors", Appl. Phys. Lett. 52, p. 634, 1988

[10] B. Kaczer, T. Grasser, J. Martin-Martinez, E. Simoen, M. Aoulaiche, Ph. J. Roussel, G. Groeseneken, "NBTI from the perspective of defect states with widely distributed time scales", Proc. IRPS 2009, pp. 55-60.

[11] H.C. Ma, J.P. Chiu, C.J. Tang, T. Wang and C.S. Chang, "Investigation of Post-NBT Stress Current Instability Modes in HfSiON Gate Dielectric pMOSFETs", Proc. IRPS 2009, pp. 51-54

[12] Reisinger, H.; Blank, O.; Heinrigs, W.; Mühlhof, A.; Gustin, W. and Schlünder, C.; "Analysis of NBTI degradation- and recovery-behavior based on ultra fast VT-measurements", Proceedings IEEE International Reliability Physics Symposium (IRPS), pp. 448-453, 2006

[13] T. Grasser, H. Reisinger, P.-J. Wagner, F. Schanovsky, W. Goes, B. Kaczer, "The Time Dependent Defect Spectroscopy (TDDS) for the Characteriza-tion of the Bias Temperature Instability", IRPS 2010, pp. 16-25

[14] H. Reisinger, O. Blank, W. Heinrigs, W. Gustin, and C. Schlünder, "A comparison of very fast to very slow components in degradation and recovery due to NBTI and bulk hole trapping to existing physical models", IEEE TDMR, Vol. 7, No. 1, p. 119 (2007)

[15] H. Kufluoglu, V. Reddy, A. Marshall, J. Krick, T. Ragheb, C. Cirba, A. Krishnan, C. Chancellor, "An Extensive and Improved Circuit Simulation Methodology For NBTI Recovery", IRPS 2010, pp. 670-675

[16] R.G. Southwick III, W.B. Knowlton, B. Kaczer, and T. Grasser, "On the thermal activation of negative bias temperature instability", 2009 IIRW final report, p. 36

[17] B. Kaczer, Ph. J. Roussel, J. Franco, R. Degraeve, L.-A. Ragnarsson, E. Simoen, G. Groeseneken, T. Grasser, H. Reisinger, "Origin of NBTI Variability in Deeply Scaled pFETs", IRPS 2010, pp. 26-32

[18] G. Math, C. Benard, J. Ogier, D. Goguenheim, "Geometry effects on the NBTI degradation of PMOS transistors", 2008 IIRW final report, pp. 60-63

[19] H. Reisinger, T. Grasser and C. Schlünder, "A study of NBTI by the statistical analysis of the properties of individual defects in pMOSFETs", 2009 IIRW final report, pp. 60-63

[20] T. Aichinger, M. Nelhiebel, T. Grasser, "Unambiguous Identification of the NBTI Recovery Mechanism using Ultra-Fast Temperature Changes", Proc. IRPS 2009, pp. 2-7

[21] B. Kaczer, V. Arkhipov, R. Degraeve, N. Collaert, G. Groeseneken, M. Goodwin, "Disorder-controlled-kinetics model for negative bias temperature instability and its experimental verification", IRPS 2005, pp. 381-387

[22] R. Fernandez, B. Kaczer, A. Nackeaerts, R. Rodriguez, M. Nafria, G. Groeseneken, "AC NBTI studied in the 1 Hz - 2 GHz range on dedicated on-chip CMOS circuits", IEDM technical digest 2006, pp.337-340

[23] K. O. Jeppson and C. M. Svensson, "Negative bias stress of MOS devices at high electric fields and degradation of MNOS devices", J. App. Phys. Vol. 48, No.5, 1977, pp. 2004-14

[24] T. Ando, A. B. Fowler and F. Stern, "Electronic properties of two dimensional systems", Rev. Mod. Phys. Vol. 54, pp.437-672, 1982

[25] ProPlus Design Solutions Inc.; www.proplussolutions.com